Determination of the Rate Coefficients for the Reactions IO + NO_2 + M (Air) → $IONO_2$ + M and $O(^3P)$ + NO_2 → O_2 + NO Using Laser-Induced Fluorescence Spectroscopy

Terry J. Dillon,[†] Mark A. Blitz,[‡] and Dwayne E. Heard*[,‡]

Max Planck Institute for Chemistry, Postfach 3060, 55020 Mainz, Germany, and School of Chemistry, University of Leeds, Leeds, LS2 9JT, United Kingdom

Received: December 4, 2005; In Final Form: March 9, 2006

Laser-induced fluorescence spectroscopy via excitation of the $A^2\Pi_{3/2} \leftarrow X^2\Pi_{3/2}$ (2,0) band at 445 nm was used to monitor IO in the presence of NO_2 following its generation in the reactions $O(^3P)$ + CF_3I and $O(^3P)$ + I_2. Both photolysis of O_3 (248 nm) and NO_2 (351 nm) were used to initiate the production of IO. The rate coefficients for the termolecular reaction IO + NO_2 + M → $IONO_2$ + M were measured in air, N_2, and O_2 over the range $P = 18-760$ Torr, covering typical tropospheric conditions, and were found to be in the falloff region. No dependence of $k(1)$ upon bath gas identity was observed, and in general, the results are in good agreement with recent determinations. Using a Troe broadening factor of $F_B = 0.4$, the falloff parameters $k_0(1) = (9.5 \pm 1.6) \times 10^{-31}$ cm^6 molecule^{-2} s^{-1} and $k_\infty(1) = (1.7 \pm 0.3) \times 10^{-11}$ cm^3 molecule^{-1} s^{-1} were determined at 294 K. The temporal profile of IO at elevated temperatures was used to investigate the thermal stability of the product, $IONO_2$, but no evidence was observed for the regeneration of IO, consistent with recent calculations for the IO−NO_2 bond strength being ∼100 kJ mol^{-1}. Previous modeling studies of iodine chemistry in the marine boundary layer that utilize values of $k(1)$ measured in N_2 are hence validated by these results conducted in air. The rate coefficient for the reaction $O(^3P)$ + NO_2 → O_2 + NO at 294 K and in 100 Torr of air was determined to be $k(2) = (9.3 \pm 0.9) \times 10^{-12}$ cm^3 molecule^{-1} s^{-1}, in good agreement with recommended values. All uncertainties are quoted at the 95% confidence limit.

Introduction

The halogen oxides, including iodine monoxide, IO, have been the subject of laboratory studies for more than 50 years.[1] Recent experimental studies have focused on the role of IO in the stratosphere[2−6] and troposphere.[7−12] Incorporating these results into atmospheric models leads to the conclusion that iodine chemistry is unimportant in the stratosphere, but within the troposphere, and in particular the marine boundary layer (MBL), iodine chemistry may be responsible for significant ozone loss.[13−19] IO has been observed at concentrations up to 7 pptv by differential optical absorption spectroscopy (DOAS) during field campaigns held at Mace Head on the Atlantic coast of Ireland, Tenerife and at Cape Grim, Tasmania.[15,20−23] Iodine atoms in the MBL are generated by the photolysis at visible wavelengths of biogenically emitted species, for example, CH_2I_2, CH_2BrI, and I_2,[23,24] which rapidly react with ozone

$$I + O_3 \rightarrow IO + O_2 \quad (3)$$

IO is rapidly photolyzed below 500 nm to generate I and O atoms but also reacts with itself or with HO_2

$$IO + HO_2 \rightarrow HOI + O_2 \quad (4)$$

$$IO + IO \rightarrow I + OIO \text{ (and other product channels)} \quad (5)$$

During the recent NAMBLEX field campaign at Mace Head, IO was found to account for up to 40% of the loss of HO_2 radicals,[25] and it was not possible to adequately model the HO_x chemistry without taking into account the significant HO_x−IO_x couplings. In this paper, we focus on a further sink of IO, namely, the recombination reaction with NO_2

$$IO + NO_2 + M \rightarrow IONO_2 + M \quad (1)$$

The atmospheric fate of the product, $IONO_2$, is rather uncertain, the possibilities being photolysis or thermal decomposition, generating I + NO_3 or IO + NO_2. The I atom channel leads to ozone destruction via reaction 3, but this is offset by photolysis of NO_3, which generates mainly NO_2 + O products and hence the production of ozone. The stability of $IONO_2$ is the key factor as to whether reaction 1 is a significant sink for both IO and NO_2 in the MBL. Recent observations of IO and I_2 at night during NAMBLEX[23] provide evidence for the reaction

$$NO_3 + I_2 \rightarrow INO_3 + I \quad (6)$$

followed by reaction 3 as providing a source of IO at night, with smaller nighttime HO_2 concentrations suggesting a greater role for reaction 1 in controlling the budget of IO.

In this paper, we report measurements of $k(1)$, using air as the bath gas, as a function of temperature and pressure and provide an upper limit for the rate of thermal decomposition of $IONO_2$ to reform IO + NO_2. The extended falloff range investigated together with the use of air as a bath gas provides data directly applicable to atmospheric models and provides an opportunity to compare with previously determined values of $k(1)$, some of which used M other than air. We also report measurements of $k(1)$ using N_2 and O_2 as the bath gas, for comparison. The method of generation of IO involved the reaction of $O(^3P)$ with alkyl iodides, and hence the observation

* Corresponding author. E-mail: d.e.heard@leeds.ac.uk.
[†] Max Planck Institute for Chemistry.
[‡] University of Leeds.

10.1021/jp057048p CCC: $33.50
Published on Web 04/15/2006

of IO temporal studies, also enabled a measurement of the rate coefficient, $k(2)$, for the reaction

$$O(^3P) + NO_2 \rightarrow O_2 + NO \quad (2)$$

Experimental Procedures

The apparatus for the study of reactions 1 and 2 using the technique of pulsed laser flash photolysis coupled with LIF detection of IO has been described previously [26,27] and is only covered briefly here. IO radicals were generated in one of two different reaction cells, both based upon a six-way cross. The first, a stainless steel cell of dimensions 15 × 15 × 15 cm and incorporating three cartridge heaters with glass-wool insulation, was used for experiments at ambient temperature and above. For lower temperatures, a second cell was used, manufactured from a single (40 × 40 × 40 cm) block of PTFE, temperatures in the range of 240 K < T < 300 K were maintained by a cooling probe (LabPlant RP-100-CD), and a curtain of N_2 was flowed over the cell windows to prevent their icing up. A calibrated thermocouple situated adjacent to the photolysis region in either cell and coupled to the heating or cooling mechanism provided temperature control to better than ±2 K.

A glass vacuum line was used for preparation, storage, and supply of the reagents used in these experiments. CF_3I and NO_2 were diluted in air and stored in (blackened) 10 L glass bulbs prior to use. The reagents were then combined with a much larger flow of N_2 or synthetic air and mixed in a steel manifold prior to entering the reaction cell through a 2 m length of PTFE tubing. All gas flows were regulated by mass flow controllers (Tylan General FC280), and the experiments were carried out under conditions of slow-flow, such that the volumetric flow rate (3000−7500 standard cubic cm^3 per min) and the laser pulse repetition frequency (prf) (1−10 Hz) ensured there was no accumulation of reaction or photolysis products in the cell. In the majority of experiments, the photolysis of O_3 at 248 nm was used to initialize the formation of IO radicals via the following sequence of reactions:

$$O_3 + h\nu \rightarrow O(^1D) + O_2 \text{ (major)} \quad (7)$$

$$O_3 + h\nu \rightarrow O(^3P) + O_2 \text{ (minor)} \quad (8)$$

$$O(^1D) + M \rightarrow O(^3P) + M \quad (9)$$

$$O(^3P) + CF_3I \rightarrow IO + CF_3 \quad (10)$$

$$O(^3P) + O_2 + M \rightarrow O_3 + M \quad (11)$$

$$O(^3P) + NO_2 \rightarrow O_2 + NO \quad (2)$$

$$IO + NO_2 + M \rightarrow IONO_2 + M \quad (1)$$

where M = synthetic air. For most experiments, 248 nm photolysis was achieved using a small excimer laser (Lambda Physik MINex, KrF mix), with a typical fluence of only 5 mJ cm^{-2} at 5 Hz prf. This method of O atom generation has a distinct advantage. The high absorption cross-section of O_3 at 248, as compared with NO_2 or CF_3I, means that the laser fluence can be kept very low, minimizing the photolysis of the reagent in excess, NO_2. O_3 was generated by passing the main flow of synthetic air over a mercury pen-lamp (Oriel 6060) prior to the reaction cell, and the concentration of O_3 in the reaction cell was estimated by direct absorption at 248 nm ($\sigma = 1.08 \times 10^{-17}$ cm^2 $molecule^{-1}$, path length $l = 40$ cm). Under all experimental conditions of total flow, cell pressure, and temperature used in this study, the observed absorbance was below the detection limit of $\ln(I_0/I) = 0.01$, corresponding to $[O_3] < 2.5 \times 10^{13}$ molecule cm^{-3}. Concentrations of all other reactants were calculated from measurements of the cell pressure and temperature, the partial pressures of reagents in the storage bulbs, and the respective mass flow-rates.

In experiments performed at Mainz, the 351 nm photolysis of NO_2 in the presence of I_2 was used to generate IO, using a pulsed XeF excimer laser

$$NO_2 + h\nu \rightarrow O(^3P) + NO \quad (12)$$

$$O(^3P) + I_2 \rightarrow IO + I \quad (13)$$

$$O(^3P) + O_2 + M \rightarrow O_3 + M \quad (11)$$

$$O(^3P) + NO_2 \rightarrow O_2 + NO \quad (2)$$

$$IO + NO_2 + M \rightarrow IONO_2 + M \quad (1)$$

where M = N_2, O_2, or synthetic air. The apparatus used for these experiments is described in Dillon et al.[28] Concentrations of NO_2 and I_2 were determined optically in a multipass absorption cell (total path length $l = 892$ cm) located upstream of the reaction cell. Attenuation of collimated light (400−560 nm) from a halogen lamp was monitored via a 0.5 m monochromator (B&M Spektronik BM50, grating 300 lines blazed at 300 nm) and diode array detector (Oriel INSTAspec 2). The observed full-width half-maximum of the Hg-line at 435.83 nm indicated a resolution of better than 0.4 nm. The concentration of I_2 was calculated from its optical absorption in the unstructured part of the spectrum at $\lambda = 490$ nm ($\sigma = 1.75 \times 10^{-18}$ cm^2) using the Beer−Lambert law. To obtain $[NO_2]$, the highly structured region of the spectra (423−442 nm) was first reduced in resolution to $\delta\lambda = 0.6$ nm using a spline function, then fit with a similarly reduced NO_2 reference spectrum.[29] The measured error in $[NO_2]$ using this method was estimated to be ∼5%.

Details of the laser excitation and fluorescence scheme are given elsewhere.[26,27] Again briefly, IO was detected at 445 nm using an excimer laser (Lambda-Physik LPX-100, 308 nm, XeCl) pumped dye laser (Lambda-Physik FL-2002, laser dye Coumarin 120), with energies up to 10 mJ per pulse. The fluorescence from IO was collected using two plano-convex lenses (Spectrasil, focal length 10 cm) and directed onto a photomultiplier (Thorn-EMI electron tubes 9813QB), the output of which was passed through a preamplifier (Stanford SR445) and processed by a boxcar integrator (Stanford SR-250) before storage on a personal computer. An interference filter (Ealing 35-3425, 470 nm), which transmitted some of the IO A−X (2,1) band, was used to discriminate against scattered laser light. The filter also discriminated against fluorescence from NO_2 at longer wavelengths, which although significantly quenched by collisions with the bath gas, would otherwise have reduced the sensitivity toward detection of IO by LIF. The IO $A^2\Pi$ state is highly predissocative, and hence, the fluorescence is not quenched by collisional quenching, and a very short boxcar integration gate was used (25 ns). To ensure that only IO was being detected, a laser excitation spectrum was recorded between 444.8 and 446 nm and was found to be entirely consistent with previously reported spectra and simulations of the IO $A^2\Pi \leftarrow X^2\Pi$ transition close to the band head of the (2,0) band.[30−32] For all kinetics studies to determine the time evolution of IO radicals, the dye laser was tuned to the band head itself at 445.054 nm. The delay between the photolysis and the probe

was computer controlled using a delay generator, and the temporal evolution of the IO signal was recorded at 200 values of this delay. The IO signal at each time delay was normalized for variations in the pulse energy of both the photolysis and the probe lasers, whose relative values were recorded using photodiodes.

Materials used with purity: NO_2 (BDH, 99.5%), CF_3I (Fluorochem, 99%), I_2 (Aldrich, 99.8%), N_2 (Air Products, Premier Grade, 99.999%), helium (Air Products, Premier Grade, 99.999%), Synthetic Air (BOC, BTCA 178, 78% N_2, 22% O_2, <1.0 ppmv (part per million by volume) CO, <300 ppmv CO_2, <0.1 ppmv NO_x, and <0.1 ppmv total hydrocarbon). I_2, NO_2, and CF_3I were purified by repeated freeze−thaw−pump cycles, whereas other reagents were used as supplied.

Results

Determination of Rate Coefficients for Reaction 1: IO + NO_2 + M → $IONO_2$ + M. The temporal evolution of IO following the photolysis of ozone (at $t = 0$) was recorded for a fixed NO_2 concentration. The IO LIF signal (S_{IO}) is given by a double-exponential function

$$S_{IO} = A[\exp(-Bt) - \exp(-Ct)] \quad \text{(E1)}$$

where A is the parameter controlling the magnitude of the IO LIF signal, given by

$$A = \alpha \frac{[O(^3P)]_0 k(10)[CF_3I]}{k(10)[CF_3I] + k(2)[NO_2] + k(11)[O_2][M] + k_{loss,O(3P)}} \times \frac{C}{C-B} \quad \text{(E2)}$$

where α is a constant of proportionality related to fluorescence detection efficiency, and $[O(^3P)]_0$ is the concentration of $O(^3P)$ atoms at $t = 0$. The parameter $k_{loss,O(3P)}$ is the total rate of loss of $O(^3P)$ other than by reaction with NO_2, CF_3I, and O_2, which is principally diffusion and pump-out from the photolysis beam, both of which are insignificant given the short lifetime of $O(^3P)$ with respect to reactions with NO_2 (2), CF_3I (10), and O_2 (11) (~300 μs at $P = 100$ Torr, $[NO_2] = 0$). The parameters B and C are pseudo-first-order rate coefficients, given by

$$B = k(1)[NO_2] + k_{loss,IO} \quad \text{(E3)}$$

$$C = k(10)[CF_3I] + k(2)[NO_2] + k(11)[O_2] + k_{loss,O(3P)} \quad \text{(E4)}$$

from which $k(1)$ and $k(2)$ were determined, respectively, by fitting (E1) to the data from a series of experiments in which S_{IO} was recorded for varying $[NO_2]$ in the range of $1-250 \times 10^{13}$ molecule cm^{-3}, while keeping $[O_3]$, $[CF_3I]$, total pressure (synthetic air), and temperature fixed. $k_{loss,IO}$ is the total rate of loss of IO other than by reaction with NO_2. The values of $k(1)$ and $k(2)$ obtained from the fits were found to be independent of $[CF_3I]$ over the range of $2-8 \times 10^{14}$ molecule cm^{-3}. In all experiments, $[O_3] < 2.5 \times 10^{13}$ molecule cm^{-3}, and from the measured laser flux and concentrations of other reagents, a maximum $[IO] = 3 \times 10^{11}$ molecule cm^{-3} was estimated, a concentration considerably lower than used in some other previous studies. The very low [IO] is made possible by the excellent sensitivity of the laser-induced fluorescence detection technique employed here.

A similar kinetic analysis was performed to obtain values of parameter B from the 351 nm photolysis of the NO_2/I_2 system

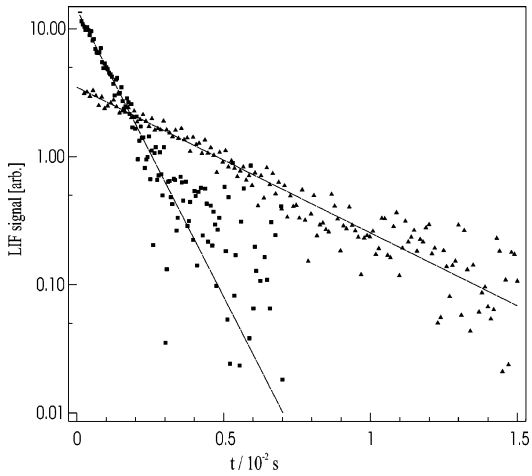

Figure 1. Semilogarithmic plot of the decay of the IO LIF signal, S_{IO}, for $[NO_2] = 1.6 \times 10^{14}$ molecule cm^{-3} (triangles) and $[NO_2] = 9.1 \times 10^{14}$ molecule cm^{-3} (squares). IO was generated following 351 nm photolysis of NO_2 in the presence of I_2 and $P = 70$ Torr (synthetic air). The rise time of the IO signal is extremely fast and was not captured. The solid line is a linear least-squares fit to the data, from which $k(1)$ is obtained (see text for details).

to generate IO. Eqs E2 and E4 are modified slightly with $k(10)[CF_3I]$ replaced by $k(13)[I_2]$. The large value of $k(13)$ and a higher concentration of $I_2 = 1.5 \times 10^{14}$ molecule cm^{-3} gives a much larger value of C and hence a very short rise time for IO, which was not captured adequately at the time resolution used. Examples of the decay of the IO LIF signal during these experiments are shown in semilogarithmic form in Figure 1 for two values of $[NO_2]$, from which it can be seen that the IO decay is described well by a single falling exponential function, from which the parameter B is obtained. From Figure 1, it can be seen that the magnitude of the initial IO LIF signal intensity is proportional to $[NO_2]$ for a constant laser fluence, as NO_2 is the source of $O(^3P)$ atoms and hence IO. As a result, there is a concurrent increase in the concentration of the photolysis cofragment, NO, and the values of B obtained in these experiments must be corrected as the term $k_{loss,IO}$ (eq E3) contains components that also scale with $[NO_2]$. The corrections to B are small (<2%), being equal to $k(5)\times([IO]/2) + k(14)\times[NO]$, accounting for the loss of IO from reactions with itself and with NO

$$IO + NO \rightarrow I + NO_2 \quad (14)$$

which both scale with $[NO_2]$. It should be stressed that only a few experiments were performed using $O(^3P) + I_2$ as the source of IO, to provide an independent measurement of $k(1)$ in the bath gases, N_2, O_2, and synthetic air.

S_{IO} was recorded for at least five different values of $[NO_2]$, while keeping other conditions fixed. From inspection of eq E3, a plot of the parameter B against $[NO_2]$ should be linear with a gradient $k(1)$, and examples are shown in Figure 2 for $P = 50$, 100, and 760 Torr (M = air), all at $T = 294$ K. The values of $k(1)$ were found to be in the falloff region, increasing with the pressure of the third body, and are listed in Table 1 and displayed in Figure 3, for $T = 294$ K. The temperature dependence of $k(1)$ was not extensively investigated in this work, with $k(1)$ determined only at a total of four temperatures for $[air] = 3.24 \times 10^{18}$ molecule cm^{-3} (~100 Torr at 294 K), as listed in Table 2.

To predict $k(1)$ beyond the range of pressures used in this study, and to estimate the high-pressure limit, $k_\infty(1)$, a Troe

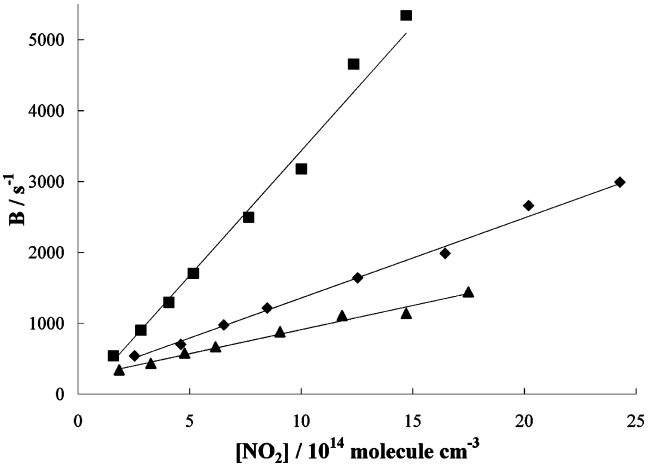

Figure 2. Parameter *B*, obtained from a fit of eq E1 to the IO temporal profiles, as a function of $[NO_2]$, for data obtained at 294 K and 50 Torr of air (triangles), 100 Torr of air (diamonds), and 760 Torr of air (squares), following 248 nm photolysis of O_3/CF_3I mixtures. Linear least-squares fits to the data are also shown, from which the rate coefficients $k(1)$ were obtained.

TABLE 1: Rate Coefficients, $k(1)$, for Reaction between IO and NO_2 at 294 K

λ/nm[a]	*M*	*P*/Torr	no. of experiments	$[NO_2]/10^{14}$ molecule cm^{-3}	$k(1)/10^{-12}$ cm^3 molecule^{-1} s^{-1}
248	air	18	6	2−20	0.44 ± 0.10
248	air	50	8	2−18	0.68 ± 0.08
248	air	100	9	1−24	1.13 ± 0.09
248	air	105	8	2−18	1.45 ± 0.15
248	air	195	9	1−10	1.95 ± 0.09
248	air	400	6	1−12	2.90 ± 0.13
248	air	600	7	1−10	3.43 ± 0.16
248	air	760	8	2−14	3.52 ± 0.19
351	N_2	70	5	1−9	1.01 ± 0.06
351	air	70	5	1−9	1.06 ± 0.06
351	O_2	70	5	1−9	1.06 ± 0.10
351	N_2	91	5	1−8	1.16 ± 0.06
351	air	91	5	1−8	1.15 ± 0.14
351	N_2	288	5	1−16	2.72 ± 0.04
351	NO_2	288	5	1−17	2.59 ± 0.09
351	N_2	390	7	2−16	2.93 ± 0.32
351	air	390	6	2−16	2.99 ± 0.34

[a] The experiments at Leeds used $\lambda = 248$ nm photolysis of O_3 as the source of O atoms that generate IO radicals in the presence of CF_3I, whereas the Mainz experiments used $\lambda = 351$ nm photolysis of NO_2 mixtures as the source of O atoms, which generate IO radicals in the presence of I_2.

formalism was adopted to parametrize the data[33−35]

$$k(1) = k_\infty F_{LH} F_B^{\,y} \qquad \text{(E5)}$$

where F_{LH} is the Lindemann−Hinshelwood factor, given by

$$F_{LH} = \frac{X}{1+X} \qquad \text{(E6)}$$

with

$$X = \frac{k_0[M]}{k_\infty} \qquad \text{(E7)}$$

and

$$y = \frac{1}{1+\left(\frac{\log X}{0.75 - 1.27 \log F_B}\right)^2} \qquad \text{(E8)}$$

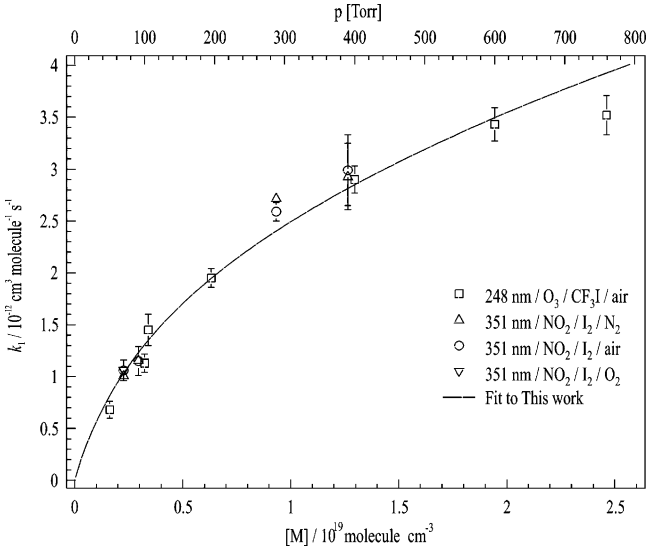

Figure 3. Pressure dependence of $k(1)$ at 294 K in air, N_2, and O_2. The experiments performed at 248 and 351 nm were performed in Leeds and Mainz, respectively. The solid line is the best fit of eq E5 to all of the data using $F_B = 0.4$, $k_0(1) = (9.5 \pm 1.6) \times 10^{-31}$ cm^6 molecule^{-2} s^{-1}, and $k_\infty(1) = (1.7 \pm 0.3) \times 10^{-11}$ cm^3 molecule^{-1} s^{-1}. The uncertainty shown for each individual rate coefficient is the 2σ error obtained from a linear-least-squares fit to second-order plots of the type shown in Figure 2.

TABLE 2: Temperature Dependence of $k(1)$ for [M](air) = 3.24×10^{18} molecule cm^{-3} (100 Torr at 294 K)

T/K	$k(1)/10^{-12}$ cm^3 molecule^{-1} s^{-1}
294	1.13 ± 0.09
263	1.65 ± 0.15
243	1.82 ± 0.1
223	2.76 ± 0.25

k_0 is the third-order rate coefficient at the low-pressure limit. We use a broadening factor of $F_B = 0.4$, which is appropriate to describe an association reaction between a linear (IO) and bent C_{2V} (NO_2) molecule in N_2 bath gas over the limited range of temperatures encountered in the atmosphere.[36] The value is similar to that used by Daykin and Wine,[37] who estimated $F_B = 0.4$, by analogy with the BrO + NO_2 reaction. There are still insufficient thermodynamic and spectroscopic data regarding the $IONO_2$ adduct to make a more informed judgment as to the optimum value of F_B for use in eq E5. We fitted eq (E5) to the values of $k(1)$ obtained at $T = 294$ K for all the third bodies used (as shown in Figure 3), from which $k_0 = (9.5 \pm 1.6) \times 10^{-31}$ cm^6 molecule^{-2} s^{-1} and $k_\infty = (1.7 \pm 0.3) \times 10^{-11}$ cm^3 molecule^{-1} s^{-1} were obtained, with uncertainties quoted at the 95% confidence level. It is reassuring that the experiments performed at Leeds, using 248 nm photolysis of $O_3/CF_3I/NO_2/M$ (M = air) mixtures, and those performed at Mainz using 351 nm photolysis of $I_2/NO_2/M$ (M = N_2, O_2, or air) mixtures, agree with one another very well.

As can be seen from Figure 3, the range of pressures used in this laser-flash photolysis study is not ideal for making direct measurements of either k_0 or k_∞. In experiments pioneered by I. W. M Smith, measurement of the rate of loss of a vibrationally excited reagent, AB ($v = 1$), has been used to estimate the k_∞ for an association reaction of AB with another species to form an adduct.[38] The rationale to this method is that following formation of the adduct, intramolecular energy redistribution will be rapid, and any dissociation of the adduct back to reagents will only yield AB ($v = 0$). Measurement of the rate of loss of AB ($v = 1$) will enable the rate of formation of the complex and hence k_∞ to be obtained. Attempts were made to measure

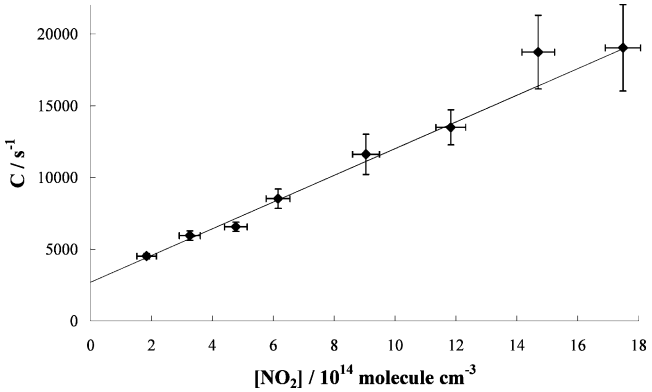

Figure 4. Parameter *C*, obtained from a fit of eq E1 to the IO temporal profiles, as a function of $[NO_2]$ for 294 K, $[CF_3I] = 6.0 \times 10^{14}$ molecule cm^{-3}, $[O_3] < 2.5 \times 10^{13}$ molecule cm^{-3}, and a total pressure of 100 Torr (air). A linear least-squares fit to the data is also shown, from which the rate coefficient $k(2)$ was obtained.

k_∞ in this manner through the measurement of the time evolution of IO ($v = 1$) to its (~4%) equilibrium concentration in the presence of NO_2, using detection by LIF in the (2, 1) band of IO at 459 nm.[30] IO($v = 1$) was observed from the $O + I_2$ reaction but was rapidly relaxed, presumably by I_2, since its removal rate was not dependent on $[NO_2]$ or the bath gas pressure. No nonequilibrium LIF signal from IO ($v = 1$) following the $O + CF_3I \rightarrow IO + CF_3$ reaction was observed, and so this method for determining k_∞ could not be used.

Reaction 2: $O(^3P) + NO_2 \rightarrow O_2 + NO$. The rate coefficient $k(2)$ for the $O(^3P) + NO_2$ reaction was obtained from analysis of the *C* parameter defined in eq E4, as a function of $[NO_2]$, while keeping $[O_3]$, $[CF_3I]$, and the total pressure constant at 50 or 100 Torr (air). Care was taken to capture a substantial number of data points during the rise of the IO signal. Figure 4 shows a plot of the *C* parameter plotted as a function of $[NO_2]$, from which a linear least-squares fit yields $k(2) = (9.3 \pm 0.9) \times 10^{-12}$ cm^3 $molecule^{-1}$ s^{-1}, in very good agreement with recommended values of $k(2)_{JPL} = 9.73 \times 10^{-12}$ cm^3 $molecule^{-1}$ s^{-1} [39] and $k(2)_{IUPAC} = (1.0 \pm 0.06) \times 10^{-11}$ cm^3 $molecule^{-1}$ s^{-1}.[36] This result demonstrates that IO, which is formed as a product of the competing reaction of $O(^3P)$ with CF_3I, may be used as a spectroscopic marker for $O(^3P)$, in much the same way that OH has been used as a marker for $O(^1D)$, following its production via reactions of $O(^1D)$ with added hydrocarbon,[40,41] or as a marker for CH_3CO [42] or C_2H_5CO,[43] following their production via the reaction $RCO + O_2$. Such markers are useful when a suitable spectroscopic method is not available for direct detection, or in the case of $O(^3P)$, when detection in air at atmospherically relevant pressures by resonance fluorescence is very difficult, as the fluorescence is heavily quenched by O_2.

Reaction (15): $IONO_2 + M \rightarrow IO + NO_2 + M$. Decomposition of the $IONO_2$ product and hence equilibration with the reagents would be manifested by a slower decay of the IO signal, which does not completely reach the instrument baseline at longer times. Despite considerable effort, no evidence for a residual IO signal at longer times was found over the temperature range of 300−450 K. Above 450 K, a rapid deterioration in the magnitude of the IO signal was observed, possibly due to decomposition of the reagents. The rate coefficient for the decomposition, $k(15)$, for the reaction

$$IONO_2 + M \rightarrow IO + NO_2 + M \qquad (15)$$

was estimated by observation of the temporal profile of IO at high temperature and comparison with a simulated IO profile using $k(15)$ as a variable parameter in a kinetic model (described in the Discussion). The simulations were performed using FACSIMILE for $T = 423$ K, $[air] = 3.24 \times 10^{18}$ molecule cm^{-3}, and $k(15) = 0$, 10, or 20 s^{-1}. The results showed that $k(15)$ must be <20 s^{-1} for the simulated IO to lie within the noise (larger at this higher temperature) of our experimental IO signal at longer times. Allan and Plane[44] performed a more extensive study of reaction 1 at higher temperatures, and using their value of $k(1) = 3.3 \times 10^{-13}$ cm^3 $molecule^{-1}$ s^{-1} at $T = 423$ K and $[M] = 3.24 \times 10^{18}$ molecule cm^{-3} and our measured upper limit of $k(15) \leq 20$ s^{-1}, the equilibrium constant $K_p = k(1)/k(15)$ was able to be estimated, and hence, $\Delta G = RT \ln K_p$. The thermodynamic data of Rayez and Destraiu[45] were used to calculate the entropy change for the forward reaction, $\Delta S(1) \approx -162$ J K^{-1} mol^{-1}, from which the reaction enthalpy change $\Delta H(15) = \Delta G + T\Delta S = 107$ kJ mol^{-1} could be calculated. This estimate of $\Delta H(15)$ is a lower limit for the dissociation energy $D_o(IO-NO_2)$, $D_o \geq 107$ kJ mol^{-1}, since we observed a rate of decomposition $k(15) <20$ s^{-1} (i.e., smaller values of $k(15)$, which are within the noise of our experiment, result in larger values of D_0). This result is consistent with values of >102 kJ mol^{-1} obtained by Allan and Plane[44] and 119 kJ mol^{-1} calculated by Rayez and Destriau.[45]

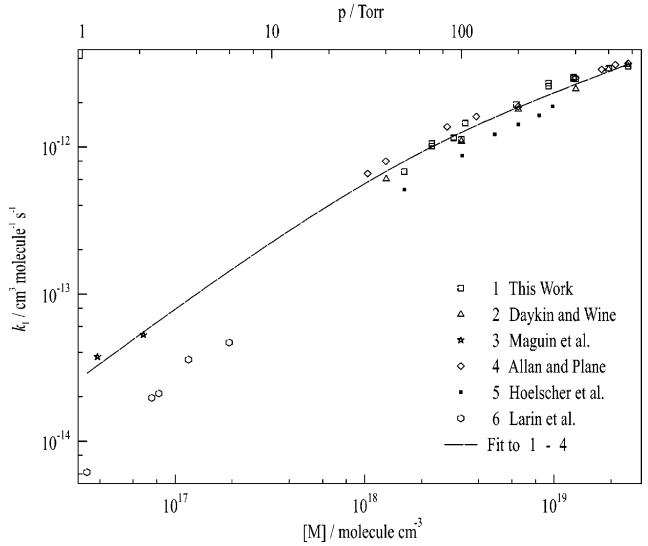

Figure 5. Variation of $k(1)$ vs [M] for room temperature, comparing the results obtained in this paper with other work from Daykin and Wine[37] (298 K, M = N_2), Maguin et al.[47] (298 K, M = He, but results corrected to M = N_2 by a factor of 2.2 as recommended by the authors), Allan and Plane[44] (301 K, M = N_2), Holscher and Zellner[49] (298 K, M = air), and Larin et al.[48] (295 K, M = O_2). The solid line is a best fit of eq E5 to all the data sets except for those of Holscher and Zellner[49] and Larin et al.[48] (see text for discussion), using $F_B = 0.4$, $k_0(1) = (10.1 \pm 0.5) \times 10^{-31}$ cm^6 $molecule^{-2}$ s^{-1}, and $k_\infty(1) = (1.4 \pm 0.1) \times 10^{-11}$ cm^3 $molecule^{-1}$ s^{-1}.

Discussion

There have been six previously published studies that report the rate coefficients for reaction 1. Jenkin and Cox[46] were the first to publish measurements of $k(1)$; however, these results were apparently perturbed by heterogeneous losses of IO in the reactor and hence are not considered further in this discussion. The results of the five subsequent studies, together with those from this work, are displayed at room temperature in Figure 5, and the falloff parameters used to describe these data are summarized in Table 3. Maguin et al.[47] (discharge flow in He coupled to mass spectrometry detection of IO) and Larin et al.[48]

TABLE 3: Comparison with Other Determinations of the Fall-Off Parameters for *k*(1) at Room Temperature

study	label	M	*T*/K	F_B	$k_0(1)^a$	$k(1)_\infty{}^b$
this paper	(1)	air, N_2, O_2[c]	294	0.4	9.5 ± 1.6	1.7 ± 0.3
Daykin and Wine[37]	(2)	N_2	298	0.4	7.7 ± 1.9	$1.55 \pm {}^{0.16}_{0.8}$
Maguin et al.[47]	(3)	He	298		3.6 ± 1.0	
		N_2	298		7.9 ± 2.2[d]	
Allan and Plane[44]	(4)	N_2	301	0.57	13 ± 2	0.65 ± 0.1
Holscher and Zellner[49]	(5)	air	298	0.6	4.1	1.1
Larin et al.[48]	(6)	O_2	300		1.8 ± 0.1	
		N_2	300		2.5 ± 1[e]	
IUPAC[36]		N_2	298	0.4	7.7 ± 2.7	1.6 ± 0.56
JPL[50]		N_2	298	0.6	5.9 ± 2.0	0.9 ± 0.1
best fit to studies 1−4 (Figure 5)				0.39	10.1 ± 0.5	1.4 ± 0.1

[a] In units of 10^{-31} cm^6 molecule^{-2} s^{-1}. [b] In units of 10^{-11} cm^3 molecule^{-1} s^{-1}. [c] The rate coefficients listed are from a fit to the data for all third bodies for experiments performed in Leeds and Mainz (Figure 3). [d] Using a relative bath gas efficiency of $He/N_2 = 2.2{:}1$.[47] [e] Using a relative bath gas efficiency of $N_2/O_2 = 1{:}0.7$.[48]

(discharge flow in O_2 with resonance fluorescence detection of I atoms) measured *k*(1) toward the low-pressure limit, but the values of k_0 obtained differed by about a factor of 2 (and more if corrections for differences in third bodies are taken into account). Larin et al.[48] speculated that a reduced third body efficiency for O_2 could account for some of this discrepancy. The three most recent studies have used laser-flash photolysis (LFP) to study reaction 1 under conditions of temperature and pressure relevant to the marine boundary layer. Daykin and Wine[37] photolyzed NO_2 at 351 nm to generate $O(^3P)$ atoms, which in the presence of I_2 produced IO, which was detected by time-resolved absorption spectroscopy to determine *k*(1), using N_2 as the third body. However, at 427 nm, the wavelength used, absorption was not specific to IO, and there was also a contribution from NO_2, and also from product species, which required a correction to *k*(1) of ∼10%. Corrections were also made for the secondary loss of IO via its self-reaction and by reaction with NO (14), which is a byproduct of NO_2 photolysis. Allan and Plane[44] subsequently used LFP (193 nm photolysis of NO_2 to yield $O(^3P)$ atoms in the presence of CF_3I) coupled to LIF detection of IO to measure *k*(1) in N_2, and these results were similarly corrected using a kinetic model for the small contribution to the IO decay from the reactions of IO with itself and NO. Holscher and Zellner[49] also used a LFP-LIF system to measure *k*(1) in air but obtained a value of *k*(1) at 295 K some 25% smaller than those obtained by either Daykin and Wine[37] and Allan and Plane.[44] Hoelscher and Zellner also suggested that a lower third body efficiency for O_2 could account for the lower values of *k*(1) they obtained in air as compared with the $M = N_2$ results of Daykin and Wine and Allan and Plane.

The literature recommendations[36,50] are largely based upon the results of Daykin and Wine,[37] and the primary motivation for the work in this current paper was to measure *k*(1) in air using a the LFP-LIF method, but under conditions where corrections to the IO profile due to its self-reaction (5) and reaction with NO (14) were unnecessary. The accuracy of fitting the biexponential function (E1) to the IO data was analyzed using a kinetic model, for which the chemical mechanism is shown in Table 4, and the initializing conditions are shown in Table 5. The base mechanism is the production of IO via the O + CF_3I reaction 10, with competing reactions of $O(^3P)$ atoms with O_2 (11) and NO_2 (2), followed by the removal of IO by reaction with NO_2 (1). Of interest is any change in the IO profile, and hence the fitted value of *k*(1), if the IO self-reaction 5 and additional reactions of I, NO, and CF_3O_2 are included. For $[NO_2] > 1 \times 10^{14}$ molecule cm^{-3} (the range used in these experiments), the change to the fitted parameters using (E1) was <1% due to the IO self-reaction and reaction with NO. In this work, the $O(^3P)$ atoms required to generate IO radicals were generated by photolysis of O_3 (rather than NO_2 as used in most of the other studies), and hence, we were able to use considerably lower concentrations of NO_2, and [NO] was small. Photolysis of CF_3I at 248 nm produces some I atoms, but the model showed that the reaction I + O_3 only produces IO at very long times ($t_{1/2}$ > 20 ms). At the higher values of NO_2 used, and at higher total pressures, this secondary production of IO is reduced further by the competing reaction I + NO_2 + M → INO_2 + M. The combined effect of including the reactions of I atoms with O_3 and NO_2 is to slightly reduce the retrieved value of *k*(1), for example, ∼10%, <2%, and <0.1% at 50, 100, and 760 Torr, respectively. Including the reaction I + CF_3O_2 (formed following photolysis of CF_3I to give CF_3, and the subsequent reaction with O_2) made no significant effect on the values of *k*(1). Therefore, we conclude that 248 nm photolyisis of $O_3/CF_3I/NO_2$ mixtures yields reliable values of *k*(1) in air and that there

TABLE 4: Iodine Reaction Scheme Used in the Kinetic Model to Investigate the Significance of Any Secondary Chemistry of IO

reaction	*k*[a]	ref
IO + NO_2 + M → $IONO_2$ + M	see text	this paper
O + NO_2 → O_2 + NO	9.73×10^{-12}	Sander et al.[50]
I + O_3 → IO + O_2	1.24×10^{-12}	Sander et al.[50]
IO + IO → OIO + I/I_2O_2	8.03×10^{-11}	Sander et al.[50]
O + CF_3I → IO + CF_3	3.72×10^{-12}	Gilles et al.[51]
O + O_2 + M → O_3 + M	6×10^{-21} [M]	Sander et al.[50]
O + I_2 → IO + I	1.4×10^{-10}	Sander et al.[50]
IO + NO → I + NO_2	2.04×10^{-11}	Sander et al.[50]
I + NO_2 + M → INO_2 + M	3×10^{-18} [M]	Sander et al.[50]
CF_3 + O_2 + M → CF_3O_2 + M	3×10^{-16} [M]	Sander et al.[50]
I + CF_3O_2 → CF_3O + IO	3.7×10^{-11}	Canosa-Mas et al.[52]
O + IO → O_2 + I	1.2×10^{-10}	Sander et al.[50]

[a] For $T = 298$ K with units of cm^3 molecule^{-1} s^{-1}.

TABLE 5: Range of Concentrations of Key Species Used to Initialize the Kinetic Model to Investigate the Significance of Secondary Iodine Chemistry

NO_2	$(0-3) \times 10^{15}$ molecule cm^{-3}
CF_3I	$(2-8) \times 10^{14}$ molecule cm^{-3}
O_2	$(6-15) \times 10^{18}$ molecule cm^{-3}
O_3[a]	$(0.5-5) \times 10^{13}$ molecule cm^{-3}
O[b]	$(0.5-5) \times 10^{12}$ molecule cm^{-3}
NO	$(0-3) \times 10^{12}$ molecule cm^{-3}
I[b]	$(2-6) \times 10^{12}$ molecule cm^{-3}
CF_3	$(2-6) \times 10^{12}$ molecule cm^{-3}

[a] $[O_3]$ calculated from the estimated 185 nm flux of the mercury photolysis lamp, the gas flow velocity in the photolysis region, and the O_2 absorption cross-section. [b] The values for [I] and [O] atoms were calculated from the range of $[CF_3I]$ and $[O_3]$ used, and the measured laser pulse energies and known absorption cross-sections were for CF_3I and O_3, respectively.

is no significant correction to be made for the effects of reactions 5 and 14, as required in some of the other studies.

The results using 248 nm photolysis obtained over a range of conditions pertinent to the MBL were complemented by the more limited dataset obtained following 351 nm photolysis of NO_2/I_2 mixtures The values of $k(1)$ obtained by this method did require small (<2%) corrections for the effects of reactions 5 and 14, but the results obtained were very similar to those using 248 nm/O_3/CF_3I. The use of two distinct photochemical generation methods (at two separate locations) increases our confidence that the values of $k(1)$ obtained in this work are not affected by secondary reactions of IO. Furthermore, the use of absorption spectroscopy to determine $[NO_2]$ in some of our experiments further reduces the scope for uncertainty. One advantage of photolyzing at 351 nm is the ability to conduct experiments in the absence of O_2, enabling values of $k(1)$ to be obtained in N_2, air, and O_2 as the bath gas. As shown in Table 1, there is a lack of any significant dependence of $k(1)$ upon bath gas identity.

The value of $k(2)$ for the reaction $O(^3P) + NO_2$ obtained from a fit to eq E2 is similarly reduced by a small amount when I atom chemistry is included in the calculation of the IO temporal profile. However, at 50 and 100 Torr, our values of $k(2)$ are in good agreement with the literature,[50] where $k(2)$ was measured in iodine-free systems, suggesting that we are overestimating the effect of the I atom secondary chemistry. One reason could be that secondary production of IO from $I + O_3$ is reduced further by reactions of I atoms and O_3 with other sinks, for example, the reactions $I + CF_3$ and $I + CF_3NO_2$ and $O_3 + CF_3$ and $O_3 + CF_3O_2$. An alternative, and more likely, explanation is that the initial $[O_3]$ was lower than the estimated value of 2.5×10^{13} molecule cm^{-3}, which was an upper limit based on the minimum optical absorbance we could measure with our system. If true, then the effect of secondary chemistry is even less significant in this study than presented previously. It is perhaps significant that Holscher and Zellner[49] employed a much larger concentration of $[O_3] = 6 \times 10^{14}$ molecule cm^{-3} in their LFP-LIF experiments to generate IO and may explain why values of $k(1)$ reported in that study were approximately 25% smaller than those obtained in this work, by Daykin and Wine[37] and by Allan and Plane,[44] because of IO production via the $I + O_3$ reaction.

Figure 5 shows that there is excellent agreement for the pressure dependence of $k(1)$ at room temperature between the experimental results of this work (M = air, N_2, and O_2), Daykin and Wine (N_2),[37] and Allan and Plane (N_2).[44] The low-pressure data of Maguin et al.,[47] which the authors recommend be corrected for bath gas efficiency (He vs N_2) also agrees well with the extrapolation of the falloff data to low pressures. The differences in the reported values of the falloff parameters, k_0 and k_∞, obtained from these data and given in Table 3, are due to the different values of the broadening factor, F_B (~0.4 in this work and by Daykin and Wine,[37] 0.57 by Allan and Plane)[44] when fitting the data. We conclude that the smaller values of $k(1)$ obtained by Larin et al.[48] (in O_2) and Holscher and Zellner[49] (in air) were more likely the result of secondary IO chemistry rather than any differences in the third body efficiencies of N_2 and O_2. Also displayed in Figure 5 is the result of a fit of eq E5 to the combined set of data from the four studies, which yielded the room-temperature falloff parameters $k_0 = (10.1 \pm 0.5) \times 10^{-31}$ cm^6 molecule^{-2} s^{-1} and $k_\infty = (14 \pm 1) \times 10^{-12}$ cm^3 molecule^{-1} s^{-1}, using $F_B = 0.4$. These overall results are in good agreement with the IUPAC recommendation[36] of $k_0 = (7.7 \pm 2.7) \times 10^{-31}$ cm^6 molecule^{-2} s^{-1} and $k_\infty = (1.60 \pm 0.56) \times 10^{-11}$ cm^3 molecule^{-1} s^{-1} using $F_B = 0.4$, but less so with the JPL recommended values[50] of $k_0 = (5.9 \pm 2.0) \times 10^{-31}$ cm^6 molecule^{-2} s^{-1} and $k_\infty = (0.9 \pm 0.1) \times 10^{-11}$ cm^3 molecule^{-1} s^{-1}, which used $F_B = 0.6$.

Conclusions

The rate coefficient $k(1)$ for the recombination reaction of IO radicals with NO_2 in the presence of synthetic air as the third body has been studied as a function of pressure (18−760 Torr) and temperature (223−294 K), using the laser-flash photolysis method combined with time-resolved detection of IO by laser-induced fluorescence. The excellent sensitivity of the LIF technique enabled very low concentrations of IO radicals to be generated by the reaction of $O(^3P)$ atoms with CF_3I, using the photolysis of low concentrations of ozone at 248 nm as the source of O atoms. A smaller number of experiments was also performed at Mainz using 351 nm photolysis of I_2/NO_2 mixtures to generate IO radicals in the bath gases N_2, O_2, and synthetic air. A kinetic model demonstrated that secondary iodine chemistry under the conditions of this study did not significantly affect the retrieved values of $k(1)$ obtained by fits to the IO temporal profiles. There were no significant differences between the values of $k(1)$ measured in air, O_2, and N_2 as the third body. The low- and high-pressure limiting falloff parameters $k_0 = (9.5 \pm 1.6) \times 10^{-31}$ cm^6 molecule^{-2} s^{-1} and $k_\infty = (1.7 \pm 0.3) \times 10^{-11}$ cm^3 molecule^{-1} s^{-1} were determined for this reaction at 294 K, using a Troe broadening factor of $F_B = 0.4$, in good agreement with recent studies performed in N_2 and with the IUPAC recommendation. The temperature dependence of $k(1)$ was also in good agreement with previous results obtained using N_2 as the third body. The results confirm that for the reaction of IO with NO_2 the third body efficiency of O_2 is very similar to that of N_2, validating previous modeling studies of iodine in the marine boundary layer that are based on the value of $k(1)$ obtained in N_2. The temporal profile of IO at elevated temperatures was used to investigate the thermal stability of the product, $IONO_2$, but no evidence was observed for the regeneration of IO, consistent with recent calculations for the IO−NO_2 bond strength being ~100 kJ mol^{-1}.

The IO profile was also used to measure the rate coefficient for the $O(^3P) + NO_2 \rightarrow NO + O_2$ reaction at 294 K and in 100 Torr of air was found to be $k(2) = (9.3 \pm 0.9) \times 10^{-12}$ cm^3 molecule^{-1} s^{-1}, in good agreement with the IUPAC and JPL recommendations.

Acknowledgment. We are grateful to the Natural Environment Research Council for the provision of a postgraduate studentship (T.J.D.) and to Mr. Ian Trought and Fr. Rosalin Karunandan for technical assistance.

References and Notes

(1) Wayne, R. P.; Poulet, G.; Biggs, P.; Burrows, J. P.; Cox, R. A.; Crutzen, P. J.; Hayman, G. D.; Jenkin, M. E.; Lebras, G.; Moortgat, G. K.; Platt, U.; Schindler, R. N. *Atmos. Environ.* **1995**, *29*, 2677.

(2) Bedjanian, Y.; LeBras, G.; Poulet, G. *J. Phys. Chem.* **1996**, *100*, 15130.

(3) Bedjanian, Y.; LeBras, G.; Poulet, G. *J. Phys. Chem. A* **1997**, *101*, 4088.

(4) Bedjanian, Y.; Le Bras, G.; Poulet, G. *J. Phys. Chem. A* **1998**, *102*, 10501.

(5) Gilles, M. K.; Turnipseed, A. A.; Burkholder, J. B.; Ravishankara, A. R. *Chem. Phys. Lett.* **1997**, *272*, 75.

(6) Gilles, M. K.; Turnipseed, A. A.; Burkholder, J. B.; Ravishankara, A. R.; Solomon, S. *J. Phys. Chem. A* **1997**, *101*, 5526.

(7) Canosa-Mas, C. E.; Flugge, M. L.; Shah, D.; Vipond, A.; Wayne, R. P. *J. Atmos. Chem.* **1999**, *34*, 153.

(8) Cox, R. A.; Bloss, W. J.; Jones, R. L.; Rowley, D. M. *Geophys. Res. Lett.* **1999**, *26*, 1857.
(9) Holscher, D.; Fockenberg, C.; Zellner, R. *Ber. Bunsen-Ges. Phys.Chem.* **1998**, *102*, 716.
(10) Harwood: M. H.; Burkholder, J. B.; Hunter, M.; Fox, R. W.; Ravishankara, A. R. *J. Phys. Chem. A* **1997**, *101*, 853.
(11) Cronkhite, J. M.; Stickel, R. E.; Nicovich, J. M.; Wine, P. H. *J. Phys. Chem. A* **1999**, *103*, 3228.
(12) Larin, I. K.; Nevozhai, D. V.; Spasskii, A. I.; Trofimova, E. M.; Turkin, L. E. *Kinet. Katal.* **1999**, *40*, 435.
(13) Solomon, S.; Garcia, R. R.; Ravishankara, A. R. *J. Geophys. Res.* **1994**, *99*, 20491.
(14) Sander, R.; Vogt, R.; Harris, G. W.; Crutzen, P. J. *Tellus* **1997**, *49*, 522.
(15) Stutz, J.; Hebestreit, K.; Alicke, B.; Platt, U. *J. Atmos. Chem.* **1999**, *34*, 65.
(16) Vogt, R.; Sander, R.; Von Glasow, R.; Crutzen, P. J. *J. Atmos. Chem.* **1999**, *32*, 375.
(17) Davis, D.; Crawford, J.; Liu, S.; McKeen, S.; Bandy, A.; Thornton, D.; Rowland, F.; Blake, D. *J. Geophys. Res.* **1996**, *101*, 2135.
(18) McFiggans, G.; Plane, J. M. C.; Allan, B. J.; Carpenter, L. J.; Coe, H.; O'Dowd, C. *J. Geophys. Res.* **2000**, *105*, 14371.
(19) McFiggans, G.; Cox, R. A.; Mossinger, J. C.; Allan, B. J.; Plane, J. M. C. *J. Geophys. Res.* **2002**, *107*.
(20) Alicke, B.; Hebestreit, K.; Stutz, J.; Platt, U. *Nature* **1999**, *397*, 572.
(21) Allan, B. J.; McFiggans, G.; Plane, J. M. C.; Coe, H. *J. Geophys. Res.* **2000**, *105*, 14363.
(22) Allan, B. J.; Plane, J. M. C.; McFiggans, G. *Geophys. Res. Lett.* **2001**, *28*, 1945.
(23) Saiz-Lopez, A.; Plane, J. M. C. *Geophys. Res. Lett.* **2004**, *31*, 19215.
(24) Carpenter, L. J.; Sturges, W. T.; Penkett, S. A.; Liss, P. S.; Alicke, B.; Hebestreit, K.; Platt, U. *J. Geophys. Res.* **1999**, *104*, 1679.
(25) Bloss, W. J.; Lee, J. D.; Johnson, G. P.; Sommariva, R.; Heard, D. E.; Saiz-Lopez, A.; Plane, J. M. C.; McFiggans, G.; Coe, H.; Flynn, M.; Williams, P.; Rickard, A. R.; Fleming, Z. L. *Geophys. Res. Lett.* **2005**, *32*, L06814.
(26) Dillon, T. J.; Heard, D. E. *J. Photochem. Photobiol., A* **2003**, *157*, 223.
(27) Gravestock, T.; Blitz, M. A.; Heard, D. E. *Phys. Chem. Chem. Phys.* **2005**, *7*, 2173.
(28) Dillon, T. J.; Karunanandan, R.; Crowley, J. N. *Phys. Chem. Chem. Phys*. **2006**, *8*, 847.
(29) Mérienne, M. F.; Jenouvrier, A.; Coquart, B. *J. Atmos. Chem* **1995**, *20*, 281.
(30) Newman, S. M.; Howie, W. H.; Lane, I. C.; Upson, M. R.; Orr-Ewing, A. J. *J. Chem. Soc., Faraday Trans.* **1998**, *94*, 2681.
(31) Western, C. M. *PGOPHER spectral simulation program written by C. M. Western.* A description of the Hamiltonian used is given in Green, M. E.; Western, C. M. *J. Chem. Phys*., **1996**, *104*, 848−864.
(32) Inoue, G.; Suzuki, M.; Washida, N. *J. Chem. Phys.* **1983**, *79*, 4730.
(33) Troe, J. *Ber. Bunsen-Ges. Phys. Chem.* **1983**, *87*, 161.
(34) Troe, J. *J. Phys. Chem.* **1979**, *83*, 114.
(35) Troe, J. *J. Chem. Phys.* **1981**, *75*, 226.
(36) Atkinson, R.; Baulch, D. L.; Cox, R. A.; Hampson, R. F.; Kerr, J. A.; Rossi, M. J.; Troe, J. *J. Phys. Chem. Ref. Data* **2000**, *29*, 167.
(37) Daykin, E. P.; Wine, P. H. *J. Phys. Chem.* **1990**, *94*, 4528.
(38) Herbert, L. B.; Sims, I. R.; Smith, I. W. M.; Stewart, D. W. A.; Symonds, A.; Canosa, A.; Rowe, B. R. *J. Phys. Chem.* **1996**, *100*, 14928.
(39) DeMore, W. B.; Sander, S. P.; Golden, D. M.; Hampson, R. F.; Kurylo, M. J.; Howard, C. J.; Ravishankara, A. R.; Kolb, C. E.; Molina, M. J. *Chemical kinetics and photochemical data for use in stratospheric modeling*; Evaluation Number 12; Jet Propulsion Laboratory, JPL Publ 97−4, 1997.
(40) Blitz, M. A.; Dillon, T. J.; Heard, D. E.; Pilling, M. J.; Trought, I. D. *Phys. Chem. Chem. Phys.* **2004**, *6*, 2162.
(41) Silvente, E.; Richter, R. C.; Zheng, M.; Saltzman, E. S.; Hynes, A. J. *Chem. Phys. Lett.* **1997**, *264*, 309.
(42) Blitz, M. A.; Heard, D. E.; Pilling, M. J. *Chem. Phys. Lett.* **2002**, *365*, 374.
(43) Romero, M. T. B.; Blitz, M. A.; Heard, D. E.; Pilling, M. J.; Price, B.; Seakins, P. W. *Chem. Phys. Lett.* **2005**, *408*, 232.
(44) Allan, B. J.; Plane, J. M. C. *J. Phys. Chem. A* **2002**, *106*, 8634.
(45) Rayez, M. T.; Destriau, M. *Chem. Phys. Lett.* **1993**, *206*, 278.
(46) Jenkin, M. E.; Cox, R. A. *J. Phys. Chem.* **1985**, *89*, 192.
(47) Maguin, F.; Laverdet, G.; Lebras, G.; Poulet, G. *J. Phys. Chem.* **1992**, *96*, 1775.
(48) Larin, I. K.; Nevozhai, D. V.; Spasskii, A. I.; Trofimova, E. M. *Kinet. Katal.* **1998**, *39*, 666.
(49) Holscher, D.; Zellner, R. *Phys. Chem. Chem. Phys.* **2002**, *4*, 1839.
(50) Sander, S. P.; Friedl, R. R.; Golden, D. M.; Kurylo, M. J.; Huie, R. E.; Orkin, V. L.; Moortgat, G. K.; Ravishankara, A. R.; Kolb, C. E.; Molina, M. J.; Finlayson-Pitts, B. J. *JPL Publ.* **2003**, 2−25.
(51) Gilles, M. K.; Turnipseed, A. A.; Talukdar, R. K.; Rudich, Y.; Villalta, P. W.; Huey, L. G.; Burkholder, J. B.; Ravishankara, A. R. *J. Phys. Chem.* **1996**, *100*, 14005.
(52) Canosa-Mas, C. E.; Vipond, A.; Wayne, R. P. *Phys. Chem. Chem. Phys.***1999**, *1*, 761.